5. MAIN INJECTOR PERFORMANCE GOALS*

5.1 Project Overview

This chapter contains a description of the design and construction schedule of the Fermilab Main Injector (FMI) Project. The technical, cost, and schedule baselines for the FMI Project have been established and may be found in the Fermilab Main Injector Title I Design Report, Revision 0, issued in August 1992. The FMI Technical Design Handbook (TDH) updates and expands upon the design and schedule for construction of all subsystem components and associated civil construction described in the Title I Design Report. The facilities described in the TDH have been designed in conformance with DOE 6430.1A, "United States Department of Energy General Design Criteria."

The purpose of the Fermilab Main Injector Project is to construct a new 150 GeV accelerator, and all required interconnections and interfaces to the existing accelerator complex, on the Fermilab site in support of the Fermilab High Energy Physics (HEP) research program. The construction of this accelerator will result simultaneously in significant enhancements to both the Fermilab collider and fixed target programs. The FMI is located south of the Antiproton Source and tangent to the Tevatron ring at the F0 straight section. The FMI will assume all duties formerly required of the Main Ring. Using the FMI reduces the background rates seen in the colliding beam detectors. The performance of the FMI, as measured in terms of protons per second delivered to the antiproton production target or total protons delivered to the Tevatron, is expected to substantially exceed that of the Main Ring. In addition the FMI will provide high duty factor 120 GeV beam to the experimental areas during collider operation, a capability which did not exist in the Main Ring.

The location, operating energy, and mode of construction of the FMI were chosen to minimize operational impacts on Fermilab's ongoing High Energy Physics program. The area in which the FMI was situated was devoid of any underground utilities which might be disturbed during construction, while the separation between the FMI and Tevatron was sufficient to allow construction concurrent with Tevatron operations. The energy capability of the FMI was chosen to match the antiproton production and Tevatron injection energies presently used in the Fermilab complex. The FMI is being built from newly constructed dipole magnets, thereby allowing a large portion of the installation process to proceed independently of Tevatron operations. The use of newly designed dipoles was also desirable from the standpoint of enhanced performance and reliability, and will result in a reduction of the operating costs by 33% relative to what would be obtained by recycling existing Main Ring magnets.

The Total Project Cost (TPC) of the FMI is estimated to be $259,300,000, including a Total Estimated Construction Cost (TECC) of $229,600,000 and $29,700,000 in associated R&D, pre-operating, capital equipment, conceptual design, and spares costs. Included within the scope of the project are all technical and civil construction components associated with the ring itself, with beam lines needed to tie the ring into the existing accelerator complex, and with modifications to the Tevatron and switchyard required to accommodate the relocated injections. The project involves the construction of 15,000 ft of tunnel enclosures, 11 service buildings, and a new 345 kV substation. Construction on the FMI project was initiated in June, 1992. Construction will be largely completed late in 1998. Design of civil construction has been done by an outside

* Last revised on March 20, 1998.

Architectural Engineering firm, Fluor Daniel, with support from the Beams Division and from Fermilab Engineering Support Section. Design of technical components has been done by Beams and Technical Division personnel.

5.1.1 Role In The Fermilab III Program

The Fermilab Main Injector is the centerpiece of Fermilab's initiative for the 1990s, known as Fermilab III. Some of the more important goals of Fermilab III are to illuminate the properties of the top quark, the most recently discovered fundamental building block of matter, to provide a factor of two increase in the mass scales characterizing possible extensions to the Standard Model, and to support new initiatives in neutral kaon physics and neutrino oscillation investigations. In order to reach these goals Fermilab is planning to attain by the end of the year 2000 a luminosity in excess of 5×10^{31} cm^{-2}sec^{-1} in the Tevatron proton-antiproton collider.

Several projects have been completed over the past four years that have resulted in a factor of 25 improvement over the initial $1.0\text{x}10^{30}$ cm^{-2}sec^{-1} design luminosity of the Tevatron collider. These include upgrades to the Antiproton Source, development of new low-β systems which have allowed the implementation of a second high luminosity interaction region, development of separators to allow multi-bunch operation, an upgrade of the linac energy from 200 MeV to 400 MeV, and the installation of cold compressors to lower the temperature of the Tevatron. As a result of these enhancements, the Tevatron operated during Run Ib with initial luminosities in the range of $1.5–2.5\times10^{31}$ cm^{-2}sec^{-1}.

Further improvements to performance require the construction of the FMI. The present bottleneck in the production of antiprotons and in the delivery of intense beams to the Tevatron is the Main Ring. The Main Ring is not capable of accelerating the quantity of protons which can be provided at injection by the 8 GeV Booster. This is for the simple reason that the aperture of the Main Ring (12π mm-mr) is about half the size of the Booster aperture (20π mm-mr). (These emittances are 95% normalized values.) As a result the Booster is typically run well below its full capability during normal operations. The restricted aperture in the Main Ring is due to perturbations to the ring which have been required for the integration of overpasses and new injection and extraction systems related to operations with antiprotons. With the 400 MeV Linac upgrade the Booster aperture at injection has increased to 30π mm-mr due to increased adiabatic damping within the new linac, and the ability to produce larger antiproton stacks has been increased. However, the mismatches between Booster/Antiproton Source and Main Ring capabilities have become even more acute. Only with the construction of the FMI will these mismatches be removed, and the full benefit to the collider and fixed target programs of the recently completed upgrade projects be realized.

The construction of the FMI will also provide beams of up to 3×10^{13} protons at 120 GeV to the experimental areas during collider runs. Such beams are envisioned as being used for detector development and for supporting fixed target experiments such as rare K decay and neutrino experiments which can benefit from the high average intensity deliverable from the FMI. The Main Ring as presently configured does not support a slow spill, nor is it felt that implementation of a high intensity slow spill in the existing ring would be feasible in light of the small machine aperture and the need to minimize backgrounds in the collider experiments.

Specifically, benefits expected from the construction of the FMI include:

1. An increase in the number of protons targeted for antiproton production from the current 4.8×10^{15}/hour to 1.2×10^{16}/hour.

2. An increase in the total number of protons which can be delivered to the Tevatron for fixed target to 6×10^{13}.
3. The ability to accelerate efficiently antiprotons originating in stacks containing more than 2×10^{12} antiprotons for injection into the Tevatron collider.
4. The ability to produce proton bunches containing as many as 3×10^{11} protons for injection into the Tevatron collider.
5. The reduction of backgrounds and dead time at the CDF and D0 detectors through removal of the Main Ring from the Tevatron enclosure.
6. Provision for slow extracted beams at 120 GeV year-round and potential development of very high intensity, high duty factor ($>1\times10^{13}$ protons/sec at 120 GeV with 34% duty factor) beams for use in high sensitivity K decay and neutrino experiments.

It is expected that with the construction of the FMI and the completion of planned improvements to the Antiproton Source the antiproton production rate will be 2×10^{11} antiprotons/hour, and that a luminosity in the range $8–20\times10^{31}\text{cm}^{-2}\text{sec}^{-1}$ will be supportable in the Tevatron collider during Run II.

5.1.2 Performance

The FMI parameter list is given in Table 5.1. It is anticipated that the FMI will perform at a significantly higher level than the existing Main Ring as measured either in terms of protons delivered per cycle, protons delivered per second, and transmission efficiency. For the most part expected improvements in performance are directly related to the optics of the ring. The FMI ring lies in a plane with stronger focusing per unit length than the Main Ring. This means that the maximum β-functions are half as large and the maximum (horizontal) dispersion only a third of the Main Ring, while vertical dispersion is nonexistent. As a result physical beam sizes associated with given transverse and longitudinal emittances are significantly reduced compared to the Main Ring. The elimination of dispersion in the rf regions, raising the level of the injection field, elimination of sagitta, and improved field quality in the dipoles all have a beneficial impact on beam dynamics. The construction of new, mechanically simpler magnets is expected to yield a highly reliable machine.

The FMI is seven times the circumference of the Booster and slightly more than half the circumference of the existing Main Ring and Tevatron. Six Booster cycles will be required to fill the FMI and two FMI cycles to fill the Tevatron. The FMI is designed to have a transverse admittance of 40π mm-mr (both planes, normalized at 8.9 GeV/c). This is a factor of three larger than that of the existing Main Ring. It is expected that the Booster will be capable of delivering a beam intensity in the range $5\text{-}7\times10^{12}$ protons per batch with 20-30π mm-mr transverse and ~0.2 eV-sec longitudinal emittance in Run II. A single Booster batch needs to be accelerated for antiproton production while six such batches are required to fill the FMI. The FMI should be capable of accepting and accelerating these protons without significant beam loss or degradation of beam quality. Yields out of the FMI for a full ring are expected to lie in the range $3\text{-}4\text{x}10^{13}$ protons ($6\text{-}8\times10^{13}$ delivered to the Tevatron for fixed target). By way of contrast, the existing Main Ring is capable of accelerating fewer than 3×10^{13} protons in 12 batches for delivery to the Tevatron.

Table 5.1. Main Injector Parameter List

Circumference	3319.419	m
Injection Momentum	8.9	GeV/c
Peak Momentum	150	GeV/c
Minimum Cycle Time (@120 GeV)	< 1.5	s
Minimum Cycle Time (@150 GeV)	2.4	s
Number of Protons	3×10^{13}	
Number of Bunches	498	
Protons/Bunch	6×10^{10}	
Max. Courant-Snyder Beta Function (β_{max})	57	m
Maximum Dispersion Function	1.9	m
Phase Advance per Cell	90	degrees
Nominal Horizontal Tune	26.425	
Nominal Vertical Tune	25.415	
Natural Chromaticity (H)	-33.6	
Natural Chromaticity (V)	-33.9	
Transverse Admittance (@ 8.9 GeV)	> 40π	mm-mr
Longitudinal Admittance	> 0.5	eVs
Transverse Emittance (Normalized)	12π	mm-mr
Longitudinal Emittance	0.2	eVs
Harmonic Number (@53 MHz)	588	
RF Frequency (Injection)	52.8	MHz
RF Frequency (Extraction)	53.1	MHz
RF Voltage	4	MV
Transition Gamma	21.8	
Superperiodicity	2	
Number of Straight Sections	8	
Length of Standard Cell	34.5772	m
Length of Dispersion-Suppressor Cell	25.9330	m
Number of Dipoles	216/128	
Dipole Lengths	6.1/4.1	m
Dipole Field (@150 GeV)	17.2	kG
Dipole Field (@8.9 GeV)	1.0	kG
Number of Quadrupoles	128/32/48	
Quadrupole Lengths	2.13/2.54/2.95	m
Quadrupole Gradient at 150 GeV	200	kG/m
Number of Quadrupole Busses	2	

The power supply and magnet system is designed to allow a significant increase in the number of 120 GeV acceleration cycles that can be run each hour for antiproton production, as well as to allow a 120 GeV slow spill with a 35% duty factor. The cycle time at 120 GeV can be as low as 1.5 seconds. This is believed to represent the maximum rate at which the Antiproton Source could stack antiprotons, and is to be compared to the current Main Ring capability of 2.4 seconds. The FMI dipole magnets are designed with twice the total cross section of copper and half as many turns as existing Main Ring dipoles. This keeps the total power dissipated in the dipoles during antiproton production at roughly the same level as in present operations while keeping the number of power supplies and service buildings low. The 344 dipole magnets are excited by 12 power supplies located in six service buildings.

With the major exception of the dipoles, existing components from the Main Ring are, for the most part, recycled. Such components specifically include quadrupoles and the radio frequency (rf) systems. The use of all 18 existing rf cavities in a ring roughly half the size of the Main Ring will support an acceleration rate of 240 GeV/sec compared to 120 GeV/sec in the present Main Ring.

5.1.3 Operational Modes

At least four distinct roles for the FMI have been identified along with four corresponding acceleration cycles for the configuration of the FMI in the absence of the Recycler. Operation of the Recycler for storing antiprotons or for cooling protons for the Collider does not require any additional cycles, but it does change some of the details of how the Collider filling operation is done. The one operation that is new with the Recycler is decelerating antiprotons which have been recovered from the Collider. The operating modes are listed in Table 5.2. More detailed descriptions of the acceleration cycles and power supply requirements are given below.

1) *Antiproton Production.* In the antiproton production mode a single Booster batch containing 5×10^{12} protons is injected into the FMI at 8.9 GeV. These protons are accelerated to 120 GeV and extracted in a single turn for delivery to the antiproton production target. As mentioned earlier, it is anticipated that with this flux of protons onto the target and expected improvements in the Antiproton Source the antiproton production rate will exceed 1.7×10^{11}/hour.

2) *Main Injector Fixed Target.* A much higher intensity, high duty factor (34%) beam can be delivered at 120 GeV with a 2.9 second cycle time. The average proton current delivered is about 2 μA (3×10^{13} protons/2.9 seconds). Running in this mode does not put any peak power demands on the power supply system beyond those imposed by the antiproton production cycle, but it does expend 67% more average power. This cycle can also be used to provide test beams to the experimental areas during collider running. In this instance it is likely that a much lower cycle rate, accompanied by a much lower average power, would satisfy experimenters' needs. Additionally, a high intensity, low duty factor beam can be delivered at 120 GeV with a 1.9 second cycle time for the production of high flux neutrino beams.

3) *Tevatron Fixed Target.* For Tevatron fixed target injection, the FMI is filled with six Booster batches, each containing 5×10^{12} protons at 8.9 GeV. Since the Booster cycles at 15 Hz, 0.4 seconds are required to fill the FMI. The beam is accelerated to 150 GeV, cogged, and extracted in a single turn for delivery to the Tevatron. The FMI is capable of cycling to 150 GeV every 2.4 seconds for short periods of time. Two FMI cycles are required to fill the Tevatron at 150 GeV at one minute intervals.

4) *Collider Operation.* The FMI operates on a 4 second, 150 GeV cycle for delivery of coalesced proton beams to the Tevatron for collider operations. A 1.45 second flattop is provided for bunch coalescing at flattop. Phase-locking to the Tevatron and synchronization of the transfer requires a few tens of milliseconds. Depending on the multi-bunch coalescing efficiency, 1, 2, 3, or 4 bunches will be accelerated per cycle. A total of 36, 18, 12, or 9 Main Injector cycles would be required, respectively, depending on the number of bunches per cycle.

The antiproton cycles are slower because of the unique rf manipulations described in section 5.5.2 and section 5.5.3. The ramps for acceleration and deceleration will be similar, and four bunches of antiprotons will be accelerated (or decelerated) per cycle.

Combinations of the above operational modes are also possible. One such example is simultaneous operation for antiproton production and high intensity slow spill. One could load the FMI with six Booster batches containing $3x10^{13}$ protons, accelerate to 120 GeV, extract one batch fast to the antiproton production target, and extract the remainder of the beam slowly over a second. This would produce slightly more than half the antiproton flux into the Source and 83% of the average MI fixed-target intensity of the dedicated scenarios listed in Table 5.2.

Table 5.2 Main Injector Cycle Parameters. "Booster Cycles" is the number of cycles required per Main Injector cycle. "MI Cycles" is the number of Main Injector cycles required to fill the Tevatron (blank if beam does not go to the Tevatron).

Purpose	Cycle Time	Flattop Time	Energy	Extraction Type	Booster Cycles	MI Cycles	MI Bunches	MI Intensity
1) Pbar Production	1.467	.04	$8 \rightarrow 120$	1 Turn	1		84	5×10^{12}
2) MI Fixed Target		.						
• Fast (1 ms spill)	1.867	.04	$8 \rightarrow 120$	Resonant	6		504	3×10^{13}
• Slow (1 s spill)	2.867	1	$8 \rightarrow 120$	Resonant	6		504	3×10^{13}
3) Tev Fixed Target	2.4	0.25	$8 \rightarrow 150$	1 Turn	6*	2	504	3×10^{13}
4) Tev Collider								
• Protons	4	1.4	$8 \rightarrow 150$	1 Turn	1–4	36–9	1-4	2.7×10^{11}–10.8×10^{11}
• Antiprotons	12	1.0	$8 \rightarrow 150$	1 Turn		9	4	varies
• Pbar Recovery	12	1.0	$150 \rightarrow 8$	1 Turn		9	4	varies

*The rise time of the existing Tevatron proton injection kicker is too slow to inject two groups of 6 batches into the Tevatron. The new short batch kicker will have a fast enough rise time provided that an appropriate pulse forming network is built.

The momentum program and the resulting total dipole bus voltage for each acceleration cycle have been calculated, using conservative extrapolations from Main Ring practice and not requiring the rf or power supplies to run close to design limits. The bus resistance is assumed to be 0.30 Ω, and the inductance is 0.67 H. The lower resistance (relative to the value of 0.32 Ω used in Title 1) allows increasing the ramp rate to 270 GeV/c/s while limiting the power supply voltage to ~11,500 V. The 2.8667 sec, 120 GeV cycle has been assumed to be run in rapid succession for calculations of rms power when designing the cooling systems and pond sizes, and for determining feeder currents and capacities. (The cycle times are required to be a multiple of the Booster 15-Hz repetition period, 0.0667 sec.)

A useful variant on the 120 GeV fixed target cycles is to fast extract one Booster batch for antiproton production before resonantly extracting to the switchyard. This approach, referred to as "mixed mode", is extremely attractive for fulfilling the demand for protons per hour. The sixth Booster batch is injected into the center of the 3.2 μsec gap that exists after the first five batches are injected. The beam is accelerated to 120 GeV, the sixth batch is extracted in a single turn to the antiproton production target, and then the remaining beam is extracted by resonant extraction to

Switchyard. For a loss of 17% in fixed target intensity the two types of operation are efficiently combined. The loss in stacking rate is about 50% when the long spill is needed but only about 20% when the short spill is used. The interleaving of single-purpose cycles is less efficient. For example, when a slow spill cycle is interleaved with an antiproton production cycle, the slow spill flux is reduced by a third, and the antiproton production is reduced by two thirds. The expected numbers of protons per hour that can be delivered in the various modes are given in Table 5.3.

The Tevatron is filled for fixed target physics by two FMI injection cycles. Average feeder power sets a limit on the frequency of the injection cycles; they can not be repeated more than a few times per Tevatron cycle. The operating limits for the magnet power supply and the rf systems are discussed in the TDH.

Table 5.3. Protons Per Hour Under Various Modes of Operation

Mode	Cycle Time (sec)	Protons/Hour AP Target	Protons/Hour Fast Spill	Protons/Hour Slow Spill
Antiproton Production	1.466	1.2×10^{16}	–	–
Fast Spill	1.866	–	5.8×10^{16}	–
Slow Spill	2.866	–	–	3.8×10^{16}
Mixed - AP + Fast Spill	2.000	0.9×10^{16}	4.5×10^{16}	–
Mixed - AP + Slow Spill	3.000	0.6×10^{16}	–	3.0×10^{16}

This table assumes 6×10^{10} protons per bunch and additional time required for bunch manipulations and turning off magnetic switch at F17 in mixed modes.

There are two accelerator physics concerns which could lead to changes in the details of the magnet ramps, especially the initial parabola. The first relates to the Main Ring experience that bunches are seriously disturbed if the synchrotron frequency approaches 720 Hz for even a few milliseconds. Although the FMI has improvements on the Main Ring magnet power supply, there is some possibility that the initial parabola might need to be slowed down to provide adequate bucket area without approaching this critical value for the synchrotron frequency. It is not anticipated that this will be a dominant concern because it will be possible to pass through the 720 Hz region quite fast from a higher value. On the other hand, it may be highly advantageous to speed up the initial parabola as much as the rf and power supplies will allow to pass the transition energy quickly. There is further discussion of transition crossing later in this section, and in the TDH.

5.2 Lattice and Performance Simulations

The Fermilab Main Injector is situated in the southwest corner of the Fermilab site. The details of its location are determined by requirements for transfers of both protons and antiprotons into the Tevatron. The MI-60 straight section is parallel to the Tevatron F0 straight section, separated from it by 11.823 m (38' 9.5") horizontally and 2.3253 m (7' 7.5") vertically. The reference point defining the plane containing the Main Injector design orbit lies at the intersection of a line from the center of the Tevatron ring and passing near F0 normal to the F0 straight section, and a line parallel to the MI-60 straight section and equidistant from the MI-60 and MI-30 straight sections. Gravity at this point defines the normal to the plane. The plane containing the Main Injector orbit dips at an angle of 0.231 milliradians (47.65") toward the southwest corner (project coordinates) of the site.

The nominal elevation of the FMI was specified in earlier design reports to be 2.332 m below the Tevatron beam. To account for the relative tilt of the Tevatron and the FMI, it is now specified that MI-52 and MI-62 are placed at this elevation. The line from MI-52 to MI-62 is offset 28.789277 m from the MI-60 straight section and parallel to it. The tilt of the FMI then places the MI-60 straight section 2.3253 m below the Tevatron beam line.

The FMI contains eight straight sections; their numbering and their functions are as follows:

MI-10 - 8 GeV proton injection
MI-22 - (unused)
MI-30 - (unused)
MI-32 - (unused)
MI-40 - proton abort
MI-52 - 150/120 GeV proton extraction; 8 GeV antiproton injection
MI-60 - FMI rf section
MI-62 - 150 GeV antiproton extraction

The straight sections are capable of beam extraction at 150 GeV. Due to the fact the ring lies 11 meters from the Tevatron, two of these (MI-52, MI-62) are required to provide injection into the Tevatron, one each for protons and antiprotons. On the opposite side of the ring two straight sections (MI-22, MI-32) are added for symmetry. MI-10 is necessary for injection of protons from the Booster, and MI-40 is placed symmetrically for the proton abort.

The FMI is designed to accelerate beams of energy 8 GeV to 150 GeV from the Booster, the Recycler, and the antiproton source. The FMI lattice has two different types of cells, the normal 17.2886-meter FODO cells and the 12.9665-meter FODO dispersion-suppressor cells. The lattice has two different length dipoles: 6 m and 4 m. Also there are three different lengths of quadrupoles: 2.13 m for normal cells, 2.95 m for dispersion suppressor cells, and 2.54 m at the boundary between the two types of cells. The dispersion suppressor cells have shorter dipoles (4 m), and match the horizontal dispersion to zero in the straight sections. The FMI lattice has fewer magnets than the Main Ring. This requires higher field dipoles and larger bending angles. The resulting sagitta in a 6 m dipole is 16 mm. The new dipoles are being built with a curvature which eliminates loss of aperture due to sagitta. A 90^o phase advance per cell is chosen, resulting in a maximum β in the cell of 58 m and a maximum η in the cell of 1.9 m. The vertical dispersion in FMI is very small. The Main Ring has maximum β and η of 110 m and 6.6 m respectively. In the lattice design, the beta function β and the dispersion η are kept small to have minimal effect on the beam size. The beam size due to transverse emittance is only 70% of what it is in Main Ring and the maximum beam size due to momentum spread is down by a factor of 3. The ring is designed to have twofold rotational symmetry. Figure 5.1 shows the lattice functions for one half the ring. The lattice function is generated by the program TEAPOT.

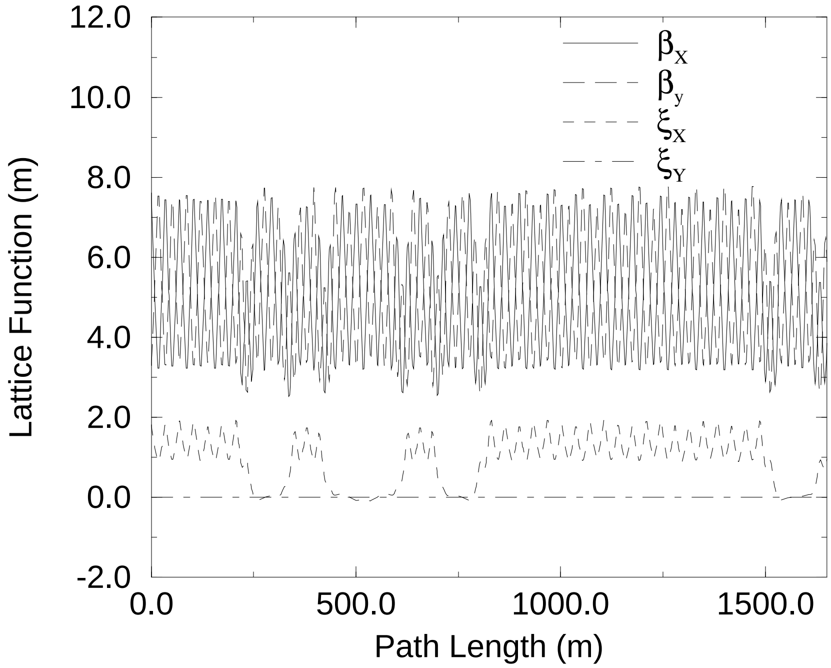

Figure 5.1. Main Injector lattice functions for one-half of the ring. The pattern shown repeats twice over the complete circumference. β_X,β_Y label the square root of the horizontal/vertical beta functions and ξ_X, ξ_Y (=0) the dispersion functions.

5.2.1 Sources of errors

Simulations have been made to investigate the performance of the Main Injector by using the code TEAPOT. Closed orbit errors and their corrections were analyzed. The extent to which field errors perturb beta functions and dispersion functions was explored. The variation of the betatron tunes, Q_x and Q_y, with respect to betatron amplitudes was recorded, and the expected dynamic aperture was predicted. All the results quoted here refer to simulations of the Main Injector at its most critical time, injection, when the beam is stored for approximately 35,000 turns at an energy of 8.9 GeV. All simulations were performed with the alignment errors of Table 5.4 and the magnetic field errors of Table 5.5.

Table 5.4. Random misalignment errors used in the Main Injector tracking simulations.

Magnet type	σ_h (mm)	σ_V (mm)	σ_{roll} (mrad)
Dipole	0.25	0.25	0.5
Quadrupole	0.25	0.25	–
Sextupole	0.25	0.25	–
Beam Position Monitor (Relative to reference orbit)	0.25	0.25	–

Although a complete explanation of all the errors listed in Table 5.4 and Table 5.5 is too lengthy to be included here, some comments are in order. Multipole field errors for dipoles are quoted in units of 10^{-4} at a displacement of one inch. "Short" dipoles will be constructed to have 2/3 the magnetic length of the "long" dipoles, 6.096 meters, at the slow extraction energy of 120 GeV. Long dipoles nominally bend the beam through an angle of $6\pi/904$ radians. At 8.9 GeV injection, the magnetic lengths of long and short dipoles are 0.3 mm longer than their nominal values, 6.096 and 4.064 meters respectively, at 120 GeV. This is reflected in the non-zero dipole multipole in the dipole ends. The average effect of this magnetic lengthening is compensated by decreasing the dipole excitation, as reflected in the non-zero dipole component of the dipole body. The remaining relative error between long and short dipoles has a significant but easily correctable effect on uncorrected closed orbit errors. Figure 5.2 shows the field profile of the Main Injector dipole field at various energies.

Table 5.5. Magnetic errors used in the 8.9 GeV simulation.

Multipole Order	Normal		Skew	
	$\langle b_n \rangle$	σ_{b_n}	$\langle a_n \rangle$	σ_{a_n}
Dipoles				
dipole	1.10	15.30	–	–
quadrupole	0.06	0.80	–	–
sextupole	-0.40	0.60	0.00	0.20
8	0.04	0.15	0.03	0.40
10	0.33	0.30	0.00	0.15
12	-0.01	0.10	-0.03	0.50
14	-0.03	0.20	0.00	0.25
Recycled Main Ring Quads (New Style)				
quadrupole	–	24.00	–	–
sextupole	0.50	2.73	0.12	1.85
8	5.85	1.02	-1.16	2.38
10	-0.10	1.12	0.42	0.47
12	-1.82	0.63	0.40	0.70
14	0.21	0.64	-0.55	0.44
16	1.41	0.64	–	–
18	-0.03	0.12	0.14	0.16
20	-0.80	0.06	0.02	0.07
Newly Built MI Quadrupole				
quadrupole	–	24.00	–	–
sextupole	-0.51	2.73	1.08	1.85
8	3.41	1.02	-2.05	2.38
10	0.03	1.12	-0.75	0.47
12	-1.49	0.63	0.43	0.70
14	0.21	0.64	–	0.44
16	1.41	0.64	–	–
18	-0.19	0.12	-0.07	0.16
20	-0.77	0.06	-0.12	0.07

Field errors for quadrupoles are quoted as the multipole field divided by the design quadrupole field, again quoted in units of 10^{-4}, at a displacement of one inch. All skew quadrupole field errors are turned off, for the convenience of the simulation, under the reasonable assumption that the linear coupling effects that they cause are readily removed in practice, using a coupling compensation scheme. Random error distributions are truncated at three standard deviations inside the TEAPOT code.

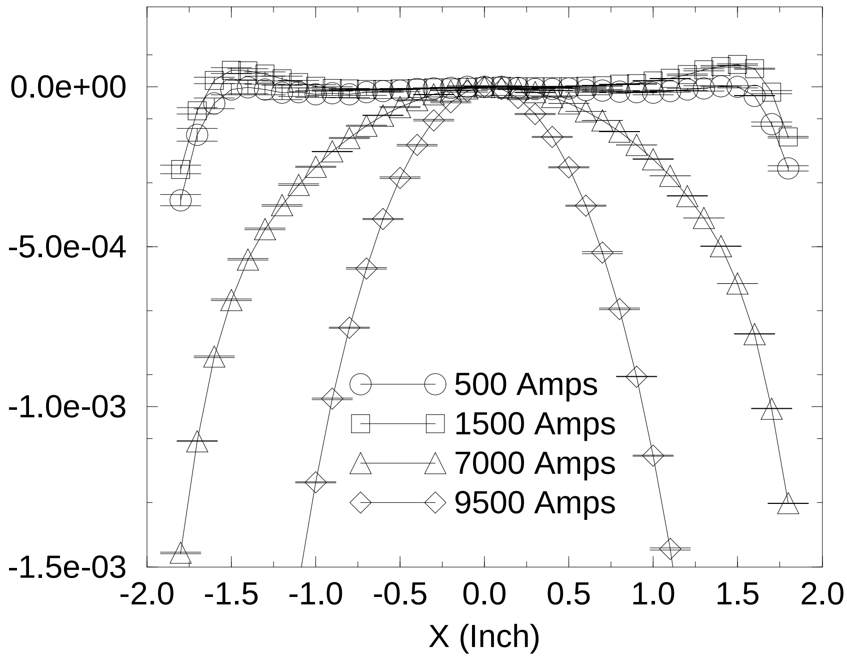

Figure 5.2. Field uniformity, ΔB/B, measured in the Main Injector dipole. The four curves correspond to 8.9, 27, 120 and 150 GeV/c excitations.

5.2.2 Closed orbit and betatron function errors

Figure 5.3 shows two superimposed histograms, representing the distribution of uncorrected horizontal and vertical closed orbit errors that are found when 19 different seeds are used to construct independent sets of random errors. The average values over all the seeds of the root mean square orbit deviation for each particular seed is 5.0 mm in the horizontal, and 3.9 mm in the vertical. In order to correct these orbits for a typical seed, the maximum required corrector strength is less than 100 μr in both the horizontal and vertical planes. A typical uncorrected closed orbit is shown in Figure 5.4, where the two traces represent horizontal and vertical displacements. After three iterations of the orbit correction scheme, the average root mean square closed orbit deviation is reduced to 4.8×10^{-4} mm in the horizontal, and 1.0×10^{-8} mm in the vertical.

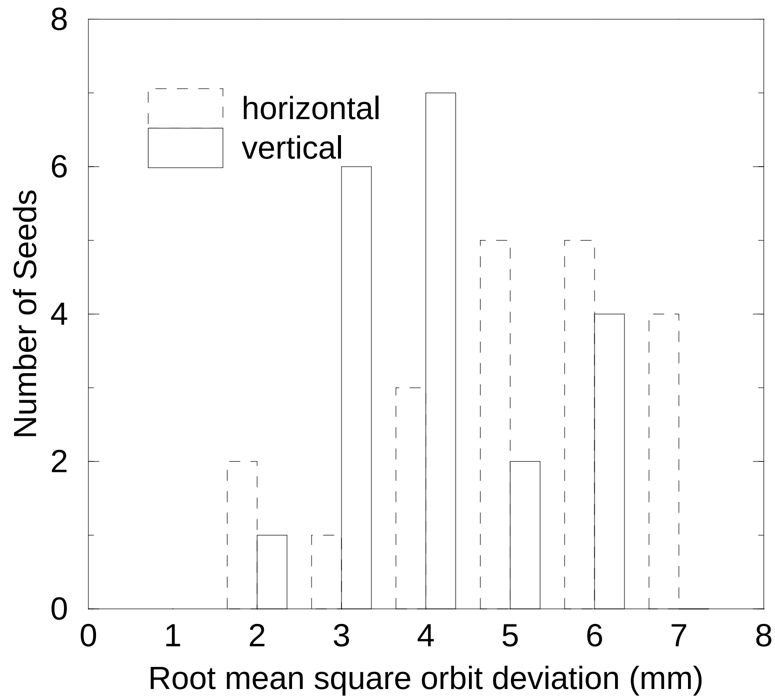

Figure 5.3. Distribution of uncorrected horizontal and vertical closed orbit errors for 19 different seeds.

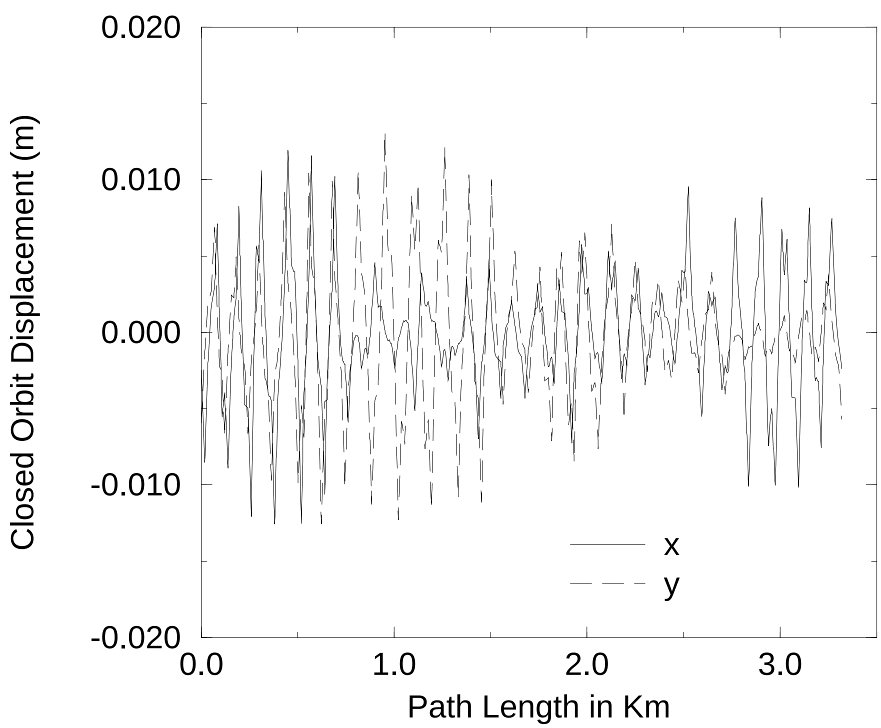

Figure 5.4. Typical uncorrected closed orbits resulting from misalignment and strength variations.

Figure 5.5 shows a plot of the typical variation of the horizontal and vertical beta functions in the Main Injector due to all sources of errors. These include dipole and quadrupole strength and misalignment errors. The main source of betatron function errors is the random quadrupole error of 2.4×10^{-3} measured in the Main Ring quadrupoles that are to be recycled, and that is conservatively assumed to be present in the newly built Main Injector quadrupoles.

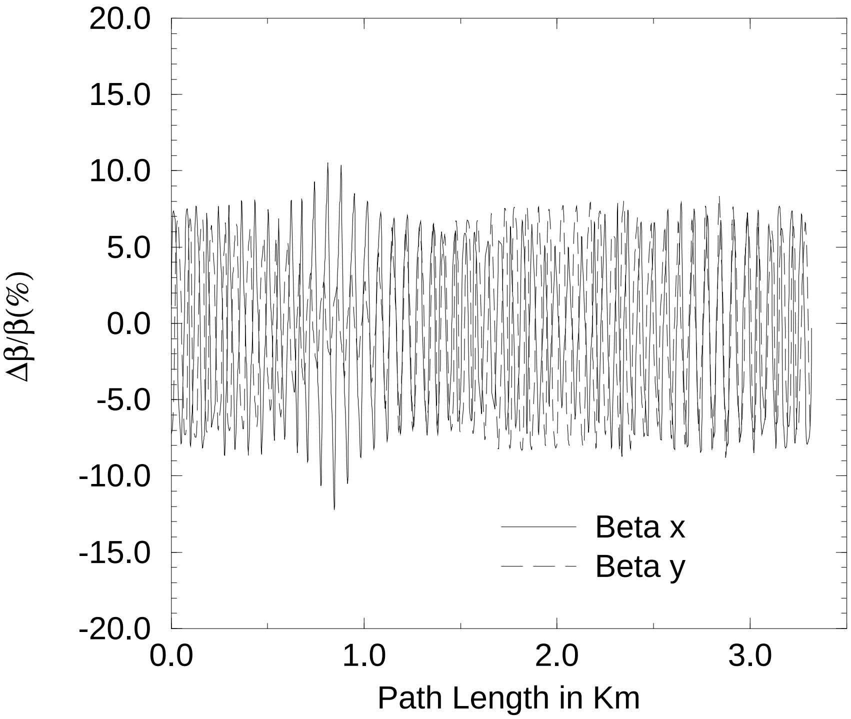

Figure 5.5. Typical beta function variation resulting from expected gradient strength and misalignment errors.

5.2.3 Tune versus amplitude and dynamic aperture results

The long-time behavior of the Main Injector at injection was tested by launching an array of particles at different amplitudes. In what follows, a test particle is labeled with an amplitude of A millimeters when, in the absence of nonlinear phase space distortions, it achieves a maximum horizontal displacement of A at a location where the horizontal beta function is 70 m. This value is chosen as a conservative maximum beta value—see Figure 5.1. The maximum vertical displacement of the same particle is 0.4 A, also at a beta of 70 m. Synchrotron oscillations were included in the simulation by launching all test particles with an amplitude of $\delta_{max} = (\Delta p/p)_{max} = 0.002$, corresponding to twice the root mean square momentum width of the beam. Net chromaticities in both planes were set to $dQ/d\delta = -5$, a conservatively large value with the correct sign to combat the head-tail instability.

Base tunes of $(Q_x,Q_y) = (26.425,25.415)$ were used in all the simulations, with unoptimized fractional tunes that were derived as follows. Slow extraction requires that the horizontal tune be moved onto the half integer without crossing a major resonance. It is conventional practice to operate near the tune diagonal, but with the tunes separated by, say, 0.01, with the horizontal tune larger to avoid crossing the coupling resonance during slow extraction. Finally, all test particles had a tune modulation amplitude in both planes of 0.01, due to non-zero net chromaticity and finite amplitude synchrotron oscillations. It is necessary to be at least this far from major resonances. Assuming that the 2/5 resonance is the resonance closest to the half integer that must be avoided, all of the above conditions are satisfied if

$$Q_y > 25.41, \qquad Q_x = Q_y + 1 + 0.01$$

The base tunes were moved an extra 0.005 away from the 2/5 resonance, without getting unduly close to the half integer.

Figure 5.6 shows the variation of horizontal and vertical tunes in the Main Injector as the amplitude of motion was increased, for a typical seed. The numbers on the tune plane plot correspond to the amplitude of a test particle, in millimeters. Points on the plot lie on a straight line up to an amplitude of about 20 mm, with the spacing between points increasing linearly. That is, both horizontal and vertical tunes depend quadratically on amplitude, for moderate amplitudes. This octupolar detuning is dominated by a combination of the systematic octupole error in the recycled Main Ring quadrupoles, and second order sextupolar effects. Points with an amplitude above 28 mm did not survive for the full 35,000 turns of the simulation, for this particular seed.

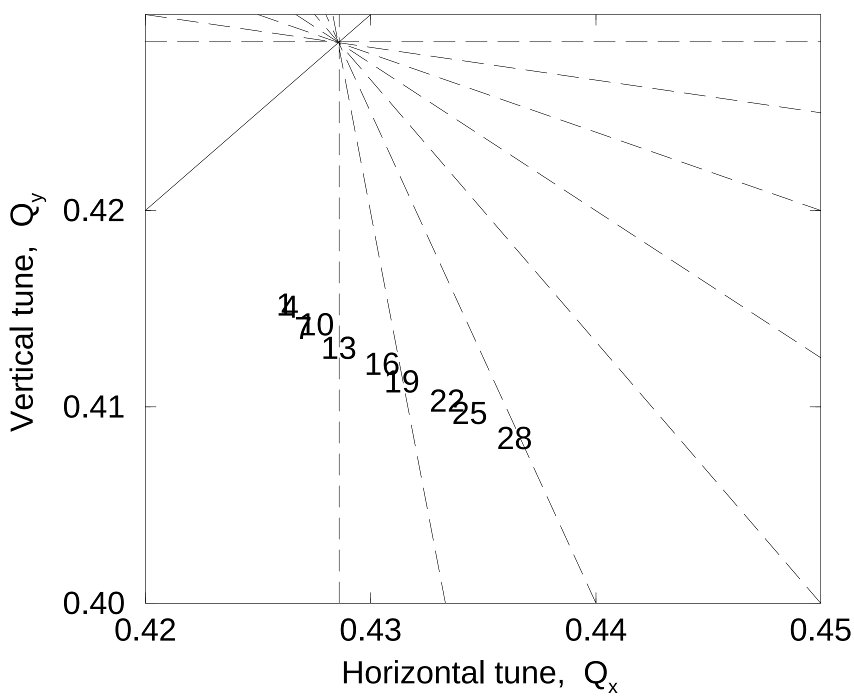

Figure 5.6. Tunes vs. amplitude in the Main Injector at 8.9 GeV/c, based on tracking for a typical seed. The numbers on the plot refer to the launch amplitude of a test particle in millimeters, and the position of the numbers indicates the tune. The lines represent resonances.

Figure 5.7 is a survival plot, displaying how many turns a particle survives in the Main Injector, as a function of its initial amplitude. Different symbols in the plot correspond to the 5 different seeds that were used. Particles that survived to the end of the simulation are plotted on a plateau at the 35,000 turn limit. If the dynamic aperture for a particular seed is defined as the amplitude of the smallest amplitude particle that does not survive for 35,000 turns, then the dynamic aperture for the Main Injector at the injection energy is predicted to be 30.6 ± 0.5 mm, corresponding to a normalized emittance of 127 π ± 4 π mm-mr.

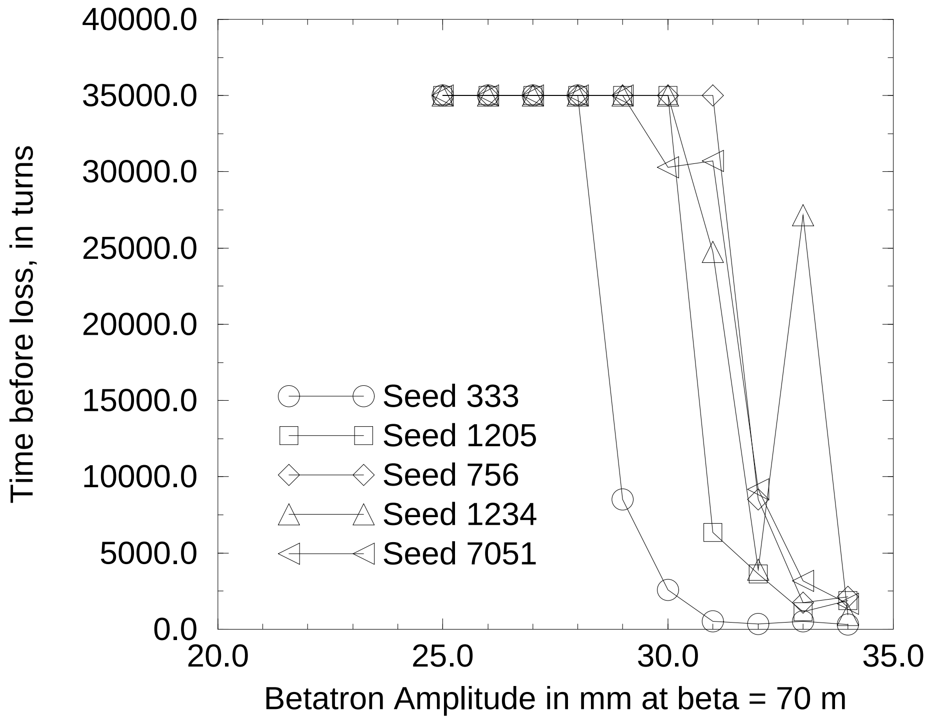

Figure 5.7. Survival plot for the Main Injector at 8.9 GeV/c. The number of turns survived, up to 35,000, is shown as a function of the launch amplitude.

5.3 Aperture

The Main Injector, as discussed above, has a dynamic aperture at injection of over 120π mm-mr, corresponding to ±30.6 mm amplitude in the horizontal plane. The injection and extraction regions, as discussed in more detail in the TDH, unfortunately require physical restrictions near the center of the aperture. While these devices limit the available physical aperture, it is still substantially greater than 40π mm-mr. To preserve the large physical aperture, good closed orbit control is required, especially at injection. To ease demands on the dipole correction elements, it is intended to induce closed orbit distortions at the extraction-device locations by intentionally misaligning quadrupoles in a controlled manner.

In the vertical plane, the dipole beam tube has an inner dimension of ~±24 mm, corresponding to an admittance of over 80π mm-mr at injection and at a β of 60 m. The injection devices will likely limit the emittance of the injected beam (but not the circulating beam) to somewhat less than this, but still provide an aperture much larger than what is required.

5.4 Transverse Emittance

The Main Injector and associated transfer lines were designed originally to accept 40π mm-mr 8 GeV proton and antiproton beams. Continuing improvements in Booster operation, however, have since reduced transverse proton emittances below 20π mm-mr. In addition, pbar emittance is also anticipated to be less than 20π mm-mr. Emittance dilution will result primarily from position and optical mismatches in transferring the beams between machines.[1]

An injection error in position and/or angle produces an oscillation which eventually decoheres and manifests itself as emittance growth in the beam. Simulations of beam transport in the 8 GeV proton line including random field and alignment errors indicate that this effect will neither be excessive nor completely negligible. For 20 error sets the injection position mismatches were found to be $\Delta x(\mathrm{rms}) = 0.39$ mm and $\Delta y(\mathrm{rms}) = 0.14$ mm—comparable to the assumed random alignment errors.[2]

At mid Q101 ($\beta_x = 10\mathrm{m}$ & $\beta_y = 60\mathrm{m}$) this translates into $< 0.5\ \pi$ growth horizontally and essentially zero growth vertically for a 20π mm-mr beam. A dispersion mismatch corresponds to a position error for off-momentum particles. However, since the transfer lines are matched to the zero dispersion of the Main Injector straight sections, emittance growth from this source is not expected to be a problem. At Q101, with a momentum spread $\Delta p/p = 10^{-3}$, dispersion would need to be mismatched by at least $\Delta\eta = 1.0$ m for emittance to grow by $0.5\ \pi$. An optical mismatch in the amplitude β will also lead to emittance dilution, but the penalty is less severe in this case than for position errors. The transfer lines are capable of matching into ±20% variations of the amplitudes from their design values. Even for a beam line-machine β mismatch as large as $\Delta\beta/\beta = 0.25$, however, transverse emittance grows by only $0.5\ \pi$ for a 20π mm-mr beam.

5.5 Longitudinal Considerations and Emittance Projections

5.5.1 Proton Acceleration and Coalescing

Proton acceleration and coalescing will be similar to the process in the Main Ring in previous collider runs. Five to seven bunches containing 6×10^{10} protons in a 0.2 eV-sec emittance will be accelerated to flat top. A flat top the bunches will be coalesced into a single bunch of 27×10^{10} protons in a 1.5 to 2.0 eV-sec emittance.

5.5.2 Antiproton Acceleration

The cooled antiproton bunches will be synchronously transferred from the Recycler to Main Injector in 2.5 MHz buckets, four bunches at a time for a total of nine transfers. The cooled antiprotons bunches will have a longitudinal emittance of 1.5 eV-sec and a typical intensity of 60×10^9 particles per bunch.

Following transfer from the Recycler, the 2.5 MHz voltage will be adiabatically raised from 2 kV (matching voltage for the transfers from the Recycler) to 60 kV. Then the antiproton bunches will be accelerated through transition to a front porch at about 25 GeV. There the bunches will be transferred to the 53 MHz rf system as follows:

a) The 2.5 MHz voltage will drop from 60-6 kV in 0. 2 msec.
b) The bunches will be rotated at 6 kV of 2.5 MHz for 1/4 of sync. period (about 100 msec).
c) The 2.5 MHz voltage will be raised again to 60 kV in 0.2 msec.
d) The bunches will be left to rotate for 1/4 of sync. period (about 30 msec).
e) The 2.5 voltage will be turned off and the bunches will be captured with 800 kV of 53 MHz.

The whole process of acceleration through transition and transfer to the 53 MHz rf system has been simulated with ESME. A longitudinal emittance blowup of 25% is predicted with no particle loss.

5.5.3 Antiproton Deceleration

The antiproton bunches that have been decelerated from 1 TeV to 150 GeV in the Tevatron will be synchronously transferred to the Main Injector, four bunches at a time for a total of nine transfers. The antiproton bunches in the Tevatron will have a typical intensity of 50×10^9 and a longitudinal emittance less than 4 eV-sec.

The pbar bunches will be decelerated to an energy close but above transition (23-25 GeV), using the 53 MHz rf system. At this point the antiproton bunches will be transferred from the 53 MHz buckets to 2.5 MHz buckets. This transfer is necessary to reduce the momentum spread of the large longitudinal emittance antiproton bunches so that they don't exceed the momentum aperture of the machine during transition crossing.

The transfer from the 53 MHz to the 2.5 MHz buckets will be take place in four steps:

a) Reduce first the 53 MHz voltage till the beam fills the bucket.
b) Turn the 53 MHz voltage off and perform a 90 degree rotation with 60 kV of 2.5 MHz and 12 kV of 5.0 MHz.
c) Go to a capture voltage of around 300 Volts of 2.5 MHz.
d) Adiabatically raise the 2.5 MHz voltage to 60 kV.

After the transfer to the 2.5 MHz rf, the antiproton bunches will be decelerated through transition with a *dp/dt* of 4 GeV/sec. The transition crossing of the antiproton bunches with 2.5 MHz has been simulated with ESME. The simulations predict a 25% emittance growth but no particle loss. After transition the rate of deceleration will be reduced to about 1.7 GeV/sec so that the existing 2.5 MHz system can continue to provide the required bucket area.

At 8.9 GeV the Main Injector will transfer cog to the Recycler, and the 2.5 MHz voltage will be adiabatically reduced until the bucket area equals the beam emittance. At this point the antiproton bunches will be synchronously transferred to the Recycler. The deceleration cycle will be about 12 sec long.

5.5.4 Transition Crossing

A set of theoretical calculations has been performed to examine the transition crossing in the Main Injector with a proton bunch of longitudinal emittance of 0.5 eV-sec and intensity of 2.7×10^{11} particles–parameters applicable to preparation of collider protons with electron cooling in the Recycler ring. Electron cooling will not be available for the early part of Run II, but it is interesting to consider the demands of the potentially small emittance beams that could be produced by electron cooling. In the initial stages of Run II, the Tevatron collider proton bunches will be formed by coalescing 5 to 7 bunches each with 6×10^{10} protons in a 0.2 eV-sec emittance. Four different transition crossing effects were examined: Negative mass instability, space charge effects, microwave instability and non-linear effects.

5.5.4.1 Negative Mass Instability

The critical coefficient c defined by W. Hardt (W. Hardt, "Gamma-transition scheme of the CPS", Proc. 9th Int. Conf. on High Energy Accelerators, Stanford 1974; also: " Transition Crossing in the Fermilab Main Ring, Past and Present" I. Kourbanis, K.Y. Ng, Proc. of the 1993 Particle Accelerator Conference, Washington , D.C., May 17-20, 1993) to give the negative mass stability limit (unstable if $c\geq1$) was calculated for the intensity above with different longitudinal emittances. The critical coefficient c is plotted as a function of longitudinal emittance in Figure 5.8. For emittances greater than 0.35 eV-sec it can be seen that $c < 1$ ($c\sim0.3$ for 0.5 eV-sec) so the beam is expected to be stable.

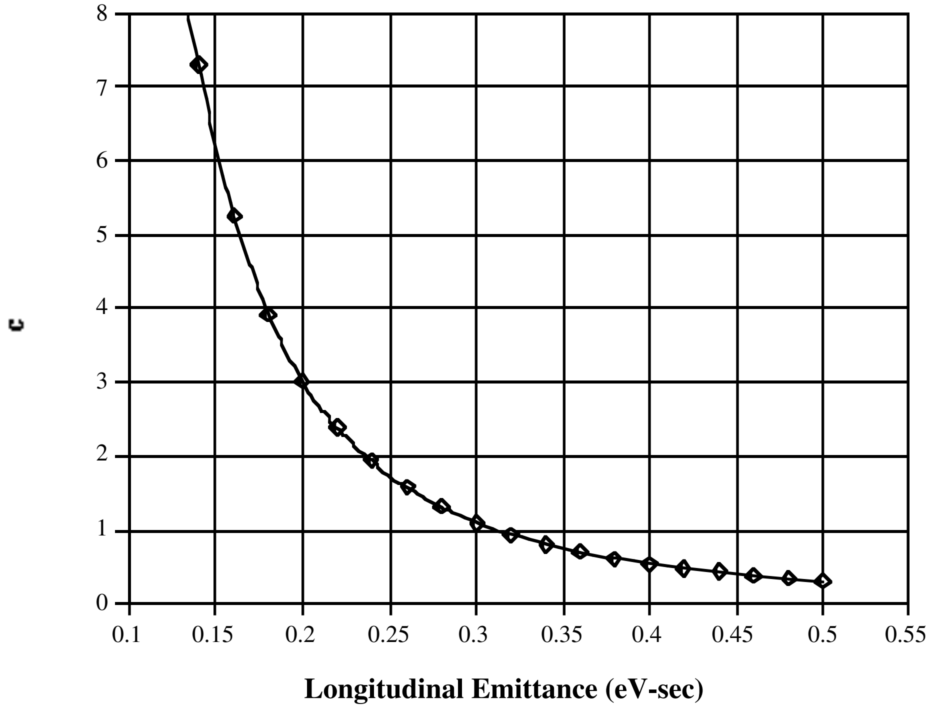

Figure 5.8. Critical coefficient c versus longitudinal emittance for $2.7\text{x}10^{11}$ ppb.

5.5.4.2 Space Charge Effects

The equations of motion near transition (with non-linearities neglected) have been solved numerically by Sorenssen and others. To evaluate the importance of the longitudinal space charge effects on the transition crossing, the space charge parameter η_0 (ratio of the space charge-force to the rf force) is calculated. The space-charge mismatch at transition is defined as the ratio of the bunch length at transition with space charge to the bunch length without space charge (and the corresponding ratio of the $\delta p/p$ at transition) as a function of the space charge parameter. The space charge mismatch at transition is not so important provided the space charge parameter is smaller than one . The calculations for the Main Injector have been done with a bunch intensity of 2.7×10^{11} ppb and with different longitudinal emittances. The results of the calculation are shown in Figure 5.9, where the space charge parameter is plotted as a function of the longitudinal emittance. Figure 5.9 shows that for longitudinal emittances greater than 0.2 eV-sec, $\eta_o < 0.5$, so space charge is not expected to be important during the transition crossing.

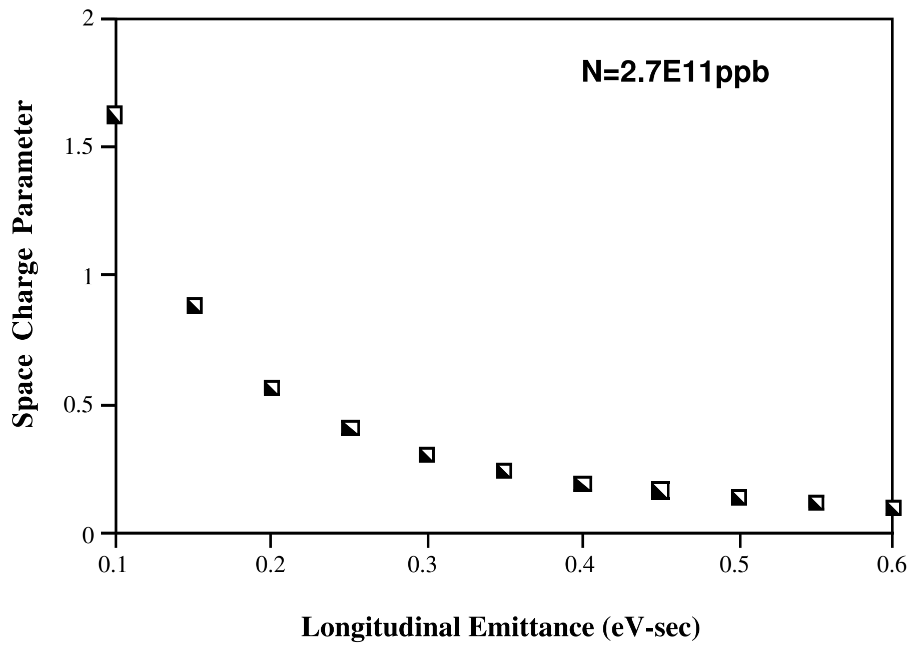

Figure 5.9. Space charge parameter η_0 versus longitudinal emittance.

5.5.4.3 Microwave Instability

The threshold for microwave instability to occur at transition for a parabolic bunch distribution is given by (J. Wei):

$$\frac{Z}{n} \leq \frac{3V\left|\cos\phi_s\right|\theta_0}{8hI} \qquad [5.1]$$

where V is the rf voltage at transition, ϕ_s the synchronous angle, h the harmonic number, θ_0 the bunch length at transition (in radians) and I is the peak bunch current. Based on the formula above, the threshold Z/n for 2.7 x 10^{11} protons as a function of the bunch emittance is plotted in Figure 5.10. For emittances greater than 0.3 eV-sec the threshold Z/n for the microwave instability is greater than the estimated Z/n for the Main Injector (less than 3 Ω), so no microwave instability is expected at transition.

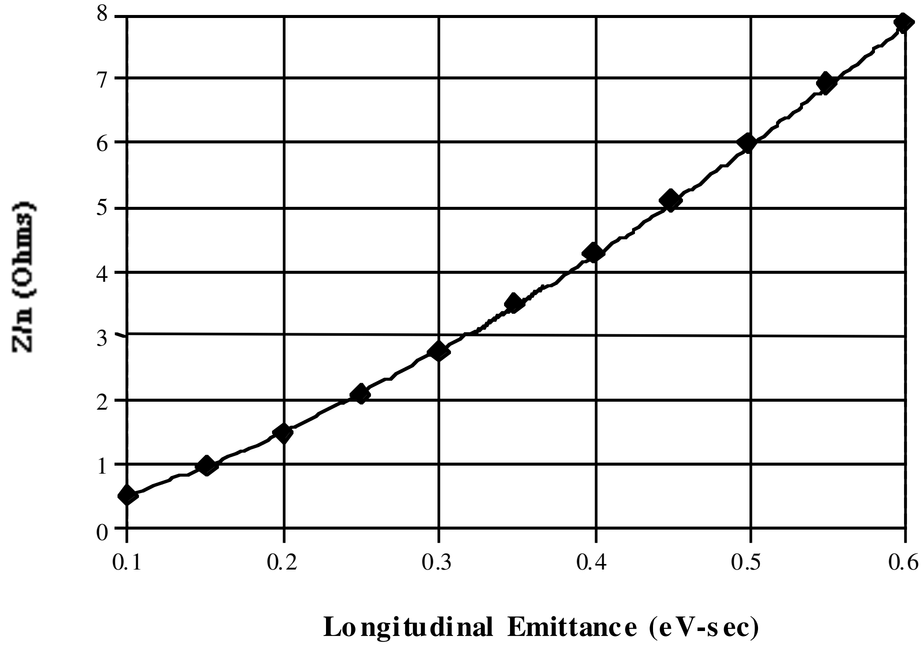

Figure 5.10. Threshold impedance Z/n versus longitudinal emittance for 2.7×10^{11} ppb.

5.5.4.4 Nonlinear Effects

Nonlinear effects are expected to dominate the transition crossing in the Main Injector under the conditions above. First the maximum $\Delta p/p$ at transition for a bunch without space charge is plotted as a function of longitudinal emittance in Figure 5.11. In these calculations a transition crossing rate $d\gamma/dt$ of 255 s^{-1} and a voltage at transition of 3.0 MV were assumed.

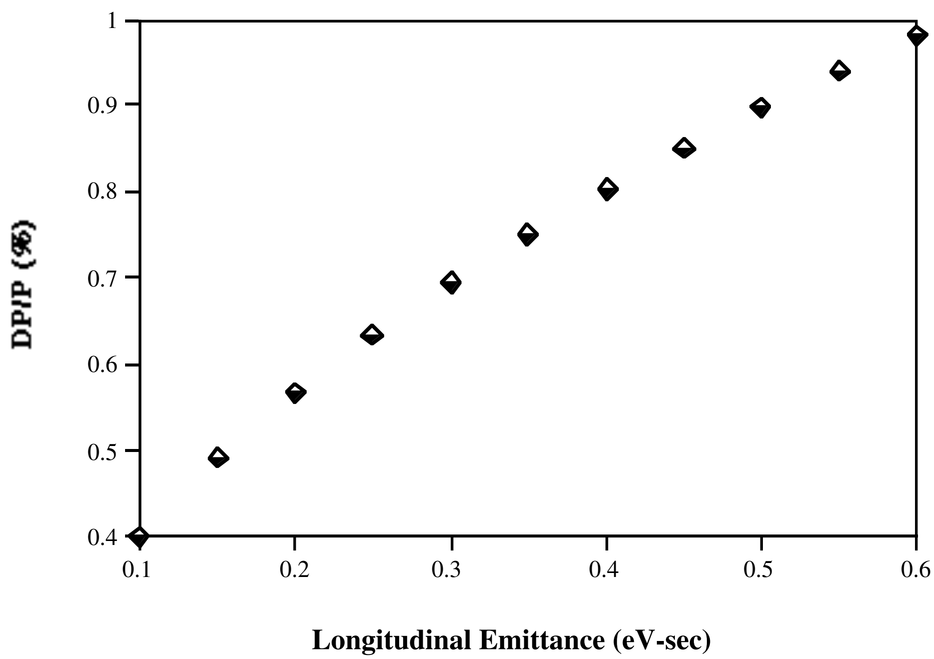

Figure 5.11. Maximum dp/p at transition as a function of longitudinal emittance.

As can be seen from Figure 5.11, for longitudinal emittances above 0.5 eV-sec, the peak excursion in Δp/p at transition is approaching the momentum aperture and beam scraping might occur. Secondly the nonlinear time (the time ΔT that it takes the particle with the largest momentum spread Δp/p to cross transition before the synchronous particle) was calculated according to the formula:

$$T_{NL} \approx \frac{(\alpha_1 + 3/2) \times \gamma_t}{\dot{\gamma}} \times \frac{dp}{p} \qquad [5.2]$$

where α_1 is the Johnsen nonlinear coefficient in the momentum compaction factor, taken to be equal to 0.65 in this case, and γ_t is the transition gamma. The results of the calculation are plotted in Figure 5.12.

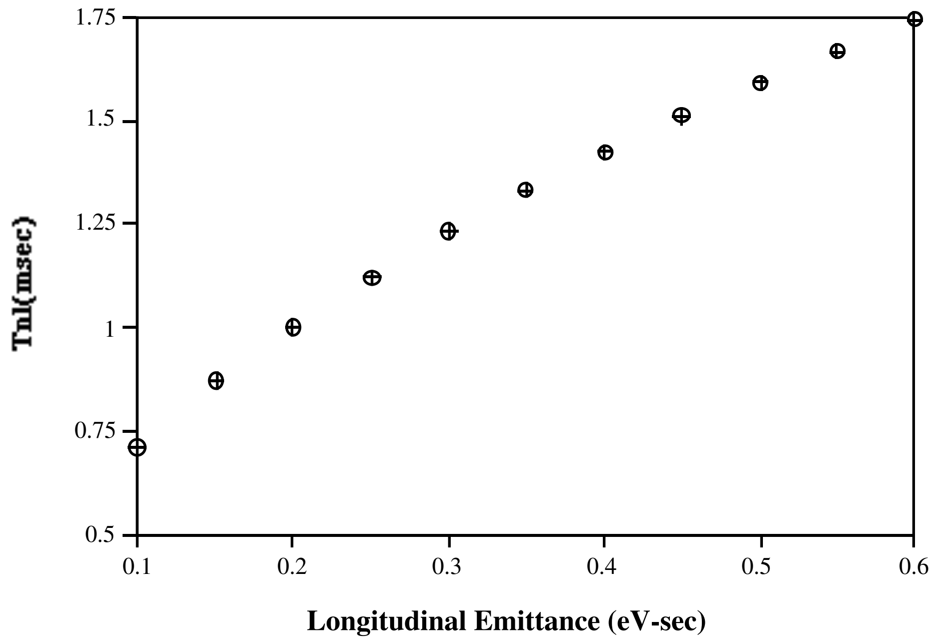

Figure 5.12. Nonlinear time as a function of the longitudinal emittance.

Figure 5.13 shows that for longitudinal emittances greater than 0.2 eV-sec the non-linear time is comparable with the characteristic time T_c (time around transition during which the particle motion is non-adiabatic), which in this case is calculated to be 2.04 msec. That will lead to the development of tails after transition, which will filament and increase the effective bunch area. The effective increase in the bunch area during the transition crossing depends on the ratio of T_{nl} to T_c (J. Wei Ph. D thesis) as follows:

$$\frac{\Delta S}{S} \approx \begin{cases} 0.76 \times \dfrac{T_{nl}}{T_c} & \text{for } T_{nl} << T_c \\ e^{\frac{4}{3} \times (\frac{T_{nl}}{T_c})} - 1 & \text{for } T_{nl} \geq T_c \end{cases} \qquad [5.3]$$

Beam loss occurs if the effective bunch area S+ΔS after transition is larger than the bucket area. The results of the formulas above for different longitudinal emittances are shown in Figure 5.13. Since T_{nl}/T_c is ranging from ~0.4 to ~0.9, neither of the two regimes applies unambiguously, and most likely, the emittance growth will fall somewhere in between the two curves. Simulations are needed to better understand the question of emittance growth in this case.

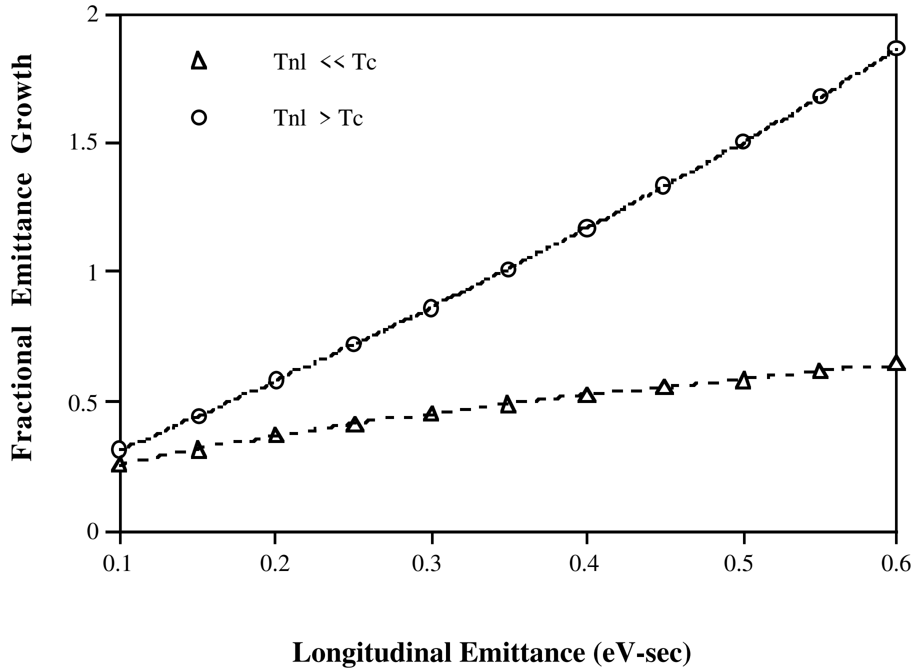

Figure 5.13. Fractional emittance growth due to nonlinear effects at transition.

A γ_t-jump of about 1.5 unit in 1 msec will decrease the nonlinear time by a factor of 6 while the characteristic time will be reduced only by a factor of 1.8, so for a given longitudinal emittance the ratio T_{nl}/T_c will become a factor of three smaller, minimizing the emittance growth and the particle loss. The gamma-t jump is a possible upgrade to the Main Injector project following initial operation for Run II.

5.5.4.5 Conclusions

The following conclusions are reached concerning transition crossing of bunches containing 2.7×10^{11} protons in a bunch of area $S_b = 0.5$ eV-s.

1. Stability against negative mass breakup requires $S_b > 0.32$ eV-s.
2. Space charge focusing mismatch at transition is not serious for $S_b > 0.2$ and is a very weak function of S_b for $S_b > 0.4$ eV-s.
3. The nominal momentum acceptance should support $S_b = 0.6$ eV-s, but potential loss at transition becomes a consideration for $S_b > 0.4$.
4. If $S_b > 0.32$ eV-s and $Z_{\|}/n < 3$ Ohm there should be no microwave instability.
5. Emittance growth from the nonlinear bunch tilt becomes a serious consideration for larger

However, the coalescing process proposed for the initial portion of Run II should not suffer from these effects in a serious way.

5.6 Impedance and instabilities

5.6.1 Impedance budget and the microwave instability

The Main Injector is a high intensity proton synchrotron. In order to control beam instabilities, it needs to be a low impedance machine. Components in the vacuum, rf, diagnostic and injection/extraction systems have been carefully analyzed, and computer models have been built. The following guidelines have been adopted in the machine design:

- The bellows are to be shielded.
- The flange gaps are to be shielded.
- The gate valves are to be shielded.
- The pump ports are to be screened.
- The transitions are to be tapered.
- The weldment gaps are to be minimized.
- The dangerous higher order modes (HOM) of rf cavities are to be damped.
- The kicker beam tubes will be coated
- The Lambertson joints are being designed with care.

There are two characteristic frequencies associated with the beam instabilities. One is the cutoff frequency of the TM01 mode of the elliptic beam tube (2"×5"), which is analytically calculable and is about 3.6 GHz. This gives an n (which is the ratio of the cutoff frequency to the revolution frequency) of 4×10^4. Another is the rms frequency of the bunch spectrum (assumed Gaussian), which is below 300 MHz and is more than an order of magnitude smaller than the cutoff. This implies that the broad-band impedance model is applicable in the analysis.

The preliminary impedance budget is listed in Table 5.6, where $Z_{\parallel}/n$ is the longitudinal impedance and $Z_{\perp}$ the transverse one. The instability thresholds at injection and extraction are also listed. The ratio of the threshold to the budget, which is sometimes called the safety margin, must be greater than unity in order to avoid microwave instabilities.

Table 5.6. Impedance Budget

Component	Number	Impedance	
		$Z_{\parallel}/n$	$Z_{\perp}$
RF cavities (HMO)		0.09	0.023
Main cavities (53 MHz)	18		
Coalescing (2.5 MHz)	5		
Coalescing (5 MHz)	1		
2nd harmonic (106 MHz)	1		
Transitions (tapered)		0.012	0.01
RF section	10		
Injection section	2		
Bellows (shielded)	552	0.37	0.67
Flange gaps (shielded)	552	-	-
Weldments	2208	0.001	0.005
Gate valves (shielded)	34	0.04	0.05
Pump ports (screened)	577	0.1	0.07
Beam position monitors	208	0.18	0.3
Kickers		0.3	0.6
proton injection (2.27 m)	3		
pbar injection (2.24 m)	2		
pbar extraction (2.2 m)	2		
Abort (2.2 m)	2		
Lambertson laminations		0.1	0.3
Lambertson joints		0.3	0.1
Lambertson-quad	12		
Lambertson-Lambertson	6		
Lambertson-dipole tube	10		
Resistive wall		0.11	0.092
Total		1.6	2.2
Instability threshold:			
At 8.9 GeV/c		39	7.9
At 120 GeV/c		8.0	16

Specific attention is needed during the bunch coalescing at 150 GeV/c. In the process of adiabatic debunching, the minimum bunch height is constrained by the machine impedance. For a bunch full height of 12 MeV, the corresponding microwave instability threshold is $Z_{\parallel}/n = 1.0\ \Omega$, which is already smaller than the budget.

Another critical stage during the cycle is the transition crossing at about 20 GeV/c, when the slip factor η tends to zero. Both analytical study and computer simulations have limited power in predicting the instability threshold. From the experiences at other high intensity proton machines (e.g., AGS at Brookhaven and PS at CERN), particle losses and emittance dilution have strong dependence on the beam intensity. However, based partly on our Main Ring experience, we do not expect the microwave instability at transition to seriously limit Main Injector performance in Run II.

5.6.2 Chromaticity and slow head-tail instability

The chromaticity in the Main Injector comes from four different sources: quadrupoles, sextupoles, eddy current in the beam tube and dipole saturation. The chromaticity model can be described as a summation of four terms:

$$\begin{pmatrix} \xi_H \\ \xi_V \end{pmatrix} = \begin{pmatrix} -33.65 \\ -32.87 \end{pmatrix} + \begin{pmatrix} 828 & 90.1 \\ -182 & -443 \end{pmatrix} \begin{pmatrix} S_F \\ S_D \end{pmatrix} + \begin{pmatrix} 0.0916 \\ -0.0859 \end{pmatrix} \frac{dp}{dt} (GeV/c/s) + \xi_{saturation} \tag{5.4}$$

It is seen that the eddy current term has a ramp rate dependence. In order to have enough room for manipulating the chromaticities in both positive and negative directions, it is necessary to have bipolar power supplies for the focusing sextupoles. (The defocusing sextupoles do not need to be bipolar.)

The head-tail growth time is inversely proportional to *Re* $Z_\perp(\omega_\xi)$, the real part of the transverse impedance at the chromaticity frequency, which is equal to $\xi\omega_o/\eta$. Table 5.7 lists the growth time of the m=±1 mode at injection for different chromaticities.

Table 5.7. Head-Tail Instability Growth Time

ξ	-33	-20	-10	-5
τ (ms)	26	27	22	17

It will be possible to adjust the crhomaticity to be negative at injection and to avoid the instability. In addition, a damper will provide stabilization even if the chromaticity has the "wrong" sign.

5.6.3 Resistive wall instability

The beam tube is made of 316L stainless steel. Its resistivity ρ is 7.4x10^{-7} Ω-m and its thickness Δ is 1.5 mm. At low frequencies near $\omega_o\Delta\nu$, where $\Delta\nu$ is the fractional tune, the skin depth δ is larger than the wall thickness. Therefore, the wall impedance is determined by the thickness.

Assuming $\Delta\nu$ = 0.4, the wall impedance would then be $Z_\perp$ = (1 + j) 19 MΩ/m. It would give a transverse coupled-bunch mode growth time τ = 1.2 ms, which is about 100 turns. The actual growth time could be longer due to other factors (chromaticity, octupoles, etc.) as observed in the Main Ring. The Main Injector damper system will suppress this instability.

5.6.4 Coupled bunch instabilities

Based on the preliminary higher-order mode (HOM) tables of the Main Injector rf cavities, the coupled bunch instability growth time is calculated and listed in Table 5.8.

Table 5.8. Coupled Bunch Instability Growth Time

Direction	Bunch Shape Mode	Growth Time (ms)	
		8.9 GeV/c	120 GeV/c
Longitudinal	m = 1	8.5	69
	m = 2	33	86
Transverse	m = 0	1900	L
	m = 1	L	L

Note: The entry "L" means Landau-damped.

The damper system should also be capable of damping these modes.

5.6.5 Transient beam loading

There are two transient beam loading effects that are of concern. One is the phase modulation due to the gap in a bunch train. For 18 cavities, each having R/Q = 80 Ω and Q =

4500, the phase modulation of several cases is listed in Table 5.9. While these phase errors are not too serious, the Main Injector will have a beam loading compensation system to reduce these effects.

Another effect is the instability driven by the fundamental mode (i.e., TM01) of rf cavities due to detuning. Feedback will be used to stabilize this potentially unstable mode.

Table 5.9. Phase Modulation from Transient Beam Loading

Case	Vrf (MV)	Io (mA)	Gap (μs)	Phase Modulation
A. 8.9 GeV/c 6 batches	0.38	430	1.7	5.3°
B. 120 GeV/c 6 batches	1	430	1.7	4.9°
C. 8.9 GeV/c 1 batch	0.38	72	9.5	20°
D. 8.9 GeV/c 5 batches	0.38	358	3.3	9.9°

5.7 Damper requirements

5.7.1 Transverse dampers

The damping process can be described as follows. Let us define a vector that represents the amplitude and phase of the collective beam oscillation:

$$\eta = \frac{x}{\sqrt{\beta}} + j\left(\frac{\alpha x}{\sqrt{\beta}} + \sqrt{\beta}x'\right) \tag{5.5}$$

where α and β are the lattice functions. When a feedback system with gain g is applied, the amplitude $|\eta|$ will be decreased. After N turns, we will have

$$|\eta(N)| = |\eta_o|\exp\left(-g\left(\frac{N}{2} + \frac{\sin(2\pi\nu(2N+1)) - \sin 2\phi_o}{4\sin 2\pi\nu}\right)\right) \tag{5.6}$$

in which $|\eta|$ and ϕ_o are the initial amplitude and phase, respectively, and ν the betatron tune. Thus, the collective amplitude damps as an exponential with a characteristic period of $2/g$ turns, but the exponential also has some minor wiggles. The transverse feedback systems in the Main Injector serve three different purposes that are described below.

5.7.1.1 Correction of injection errors.

If there is a position error x_c at injection, the decoherence due to chromaticity is described by $A = (x_c - \bar{x})/x_c$, where x_c is the centroid of the particle distribution in a bunch. The decoherence factor can be calculated by

$$A(N) = 1 - \exp\left\{-2\left[\frac{\xi \cdot \left(\frac{\sigma_p}{p}\right)}{\nu_s}\sin(\pi\nu_s N)\right]^2\right\} \quad [5.7]$$

in which ξ is the chromaticity, σ_p/p the rms relative momentum spread, ν_s the synchrotron tune, and *N* the number of turns after injection. Table 5.10 lists the maximum value of *A* as a function of ξ, which occurs when $N = 1/2\nu_s$. It is seen that, for a large chromaticity, the damping time of the injection damper must be shorter than half of the synchrotron period in order to avoid any significant emittance dilution due to decoherence.

Table 5.10**.** The Decoherence Factor

ξ	33	20	10	5
A_{max}	1	0.99	0.72	0.27

5.7.1.2 2. Damping of the resistive wall instability:

Because this is a fast beam blowup, a feedback system with a large gain is needed. The maximum bandwidth is determined by the batch separation.

5.7.1.3 3. Damping of the coupled-bunch instability:

In order to be able to damp the coherent oscillation of each individual bunch, this feedback system needs a wide bandwidth. It is planned to build two feedback systems in each transverse plane. System A has high power and medium bandwidth for correcting injection errors, while System B has low power and wide bandwidth for damping the resistive wall and coupled-bunch instabilities. The specifications are listed in Table 5.11.

Table 5.11**.** Specifications of Transverse Feedback Systems

Feedback system	A	B
Purpose(s)	Injection errors	Resistive wall instability Coupled bunch instability
Features	High power Medium gain Medium bandwidth	Low power Large gain Wide bandwidth
Gain	0.04	0.1
Damping time (turns)	50	20
Correction (mm)	±3	±0.3
Kick angle (μrad)	6	1.5
Kicker length (m)	1.4	1.4
Kicker voltage (V/mm)	160	400
Total voltage (V)	±480	±120
Kicker power (kW)	5	0.3
Bandwidth (MHz)	4	53

The simplest implementation of a feedback system consists of a pickup and a kicker, which are (n+1/2)π apart in phase advance. But this simple scheme is sensitive to tune variations, closed orbit errors, and the initial phase of the bunch at the pickup/kicker.

An improved version is as follows:

1. Two pickups taken together determine both x and x', thereby eliminating the sensitivity to initial phase and tune variations.
2. Two-turn (or multiple-turn) measurement will reject the closed orbit signal.
3. Two kickers, which can get rid of the initial phase dependence, will (in principle) provide almost exact orbit correction within one turn.

A new transverse feedback system, which has both high power (6 kW) and wide bandwidth (53 MHz), has been built for the Main Ring and will be used in the Main Injector.

Another important consideration for dampers is the noise level of the system. This may not be a problem for the Main Injector because of its short cycle time, but it is critical for any proton storage ring. The consequence of noise in the feedback system is the possible emittance dilution. The emittance growth due to the feedback noise can be described by

$$\frac{d\varepsilon}{dt} = \varepsilon_o \left\{ 0.64 f_o \left(\frac{x_N}{\sigma_x} \right)^2 \Delta\nu^2 \right\} \qquad [5.8]$$

in which ε_O is the initial emittance, f_O the revolution frequency, x_N the equivalent noise level at the pickup, σ_x the rms beam size, and $\Delta\nu$ the total tune spread. It is interesting to note that the growth rate is independent of the gain and is proportional to the square of the tune spread (which is somewhat contrary to one's intuition). The theoretical limit of the pickup resolution due to thermal and electronic noise, Δx, is also calculable. In designing a feedback system, Δx must be smaller than x_N, which is determined by a specified allowable growth rate $d\varepsilon/dt$.

5.7.2 Longitudinal dampers

Passive mode dampers will be used on the Main Injector cavities (which are being reused from the Main Ring). In addition, phase feedback will be used as necessary to damp dipole oscillations. Quadrupole feedback will be used for the m=0 mode.

5.8 RF Systems and Beam Loading Compensation

The 18 existing 53 MHz Main Ring rf cavities will be installed in straight section MI-60 and operated at harmonic number 588. The operating levels below transition are determined by an interplay between cycle time, bucket area, and synchrotron frequency. Since the FMI must accelerate antiprotons as well as protons, a degree of simplicity and system flexibility will be achieved by placing the cavities at spacings that are multiples of one-half the rf wavelength. The 180° spacing of accelerating cavities will simplify the rf signal distribution (fan-out/fan-back) system as well as providing simpler choices for coalescing stations.

A bucket area of at least 0.2 eV sec is required to accept beam out of the Booster. Historically, it has been necessary to keep the synchrotron frequency in the Main Ring below 720 Hz to avoid resonance with power supply ripple at the twelfth harmonic of the line frequency. The rf system has the capability of generating enough voltage at injection to produce a 1.0 eV sec bucket area at injection, where the limit of 150 kV per cavity is set by the tendency of the tuners to spark because they are close to parallel resonance. In this mode the synchrotron frequency lies well above 720 Hz at injection and descends rapidly, crossing 720 Hz when the beam energy is about

15 GeV. At the frequency for transition energy the cavities are capable of producing 240 kV each, so that 4.0 MV are available even with one cavity inoperative. If the rf system has more than a 50% duty factor, it is not possible to maintain the 4 MV level all the way to top energy because of cavity heating. Operational experience will dictate the exact ramp scenario that is used.

One limitation of the existing Main Ring rf system is the power that it can deliver. The present requirements are 70 kW per cavity with the increased beam intensity provided by the Linac upgrade. The FMI will require 112 kW for accelerating the full intensity at 240 GeV/sec, which is excessive for rf amplifier reliability using the present Main Ring rf system. Provision in the original cavity design allowed for a second amplifier to be installed on the cavity. This choice, while possible, places additional amplifier components in the enclosure, thus increasing maintenance. To overcome this limitation, a new 200 kW power amplifier is placed in the tunnel with a 4 kW rf driver and 30 kV series tube modulator in the equipment gallery. R&D development of a 200 kW rf power amplifier and a 4 kW driver has been completed. Tevatron style 500 volt programmable grid and screen supplies are used for dc biasing. Rf drive is be provided by a solid-state 4 kW rf driver coupled to the final tube cathode.

More than 200 kW of output power has been achieved with the new amplifiers. Reliability testing is being done in a test station and in an active accelerating station in the Main Ring rf System. Operation in a Main Ring Station since May 15, 1994 without failure, has given us encouragement that the design is sound.

The transient beam loading from 6×10^{10} protons per bunch will require about 1.25 amp delivered to the cavities, supplied by 15 A (12:1 cavity step-up ratio) of rf current generated by the power amplifier. A 200 kW rf power amplifier operated at a dc plate voltage of 20 kV will produce a peak rf current of approximately 21 A. The 40% surplus initial current capability will insure adequate operating lifetime as the power tube ages.

In the present Main Accelerator rf systems, two 30 kV anode power supplies provide dc power to 18 rf stations. Nine stations are powered by each anode supply. With 200 kW amplifiers, only six stations can be powered by a MR anode supply. One additional anode supply will be provided. The two existing MR anode supplies will be rebuilt at the MI-60 location when the Main Ring is decommissioned. Design improvements proven to increase reliability in a similar supply used in the Tevatron rf systems will be implemented. This will make the Main Injector anode supplies similar to the Tevatron supply. Uniformity of the systems will both ease maintenance and provide consistent safety requirements in the two systems.

The FMI will use the 2.5 and 5.0 MHz coalescing cavities from the Main Ring to prepare intense bunches for collider loading; no significant modifications are required. The system consists of five 2.5 MHz ferrite loaded cavities producing 12 kV per cavity and one 5.0 MHz cavity producing 15 kV. These cavities are driven with solid state amplifiers which will be located in the MI-60 Service Building. Because the harmonic number for 2.5 MHz is 28 in the FMI compared to its Main Ring value of 53, the system will provide 1.4 times the bucket height available in the Main Ring. For longitudinal emittance of 0.15 eVs, about 30 kV of 2.5 MHz rf is required, so there is substantial reserve in this system. The FMI will also use a 15 kV, 106 MHz cavity from the Main Ring. It is used to linearize the 53 MHz bunch rotation in the procedure called snap coalescing.

The four operating modes of the Main Injector are listed below.

Table 5.12. Operating Modes of the Main Injector.

Energy	Mode	Beam	Extraction
120 GeV	Antiproton Production	1 batch	1 turn
120 GeV	Slow Spill	6 batch	1 sec
150 GeV	Tevatron Fixed Target	6 batch	1 turn
150 GeV	Collider, 36 on 36	11 bunch	1 turn

For antiproton production and fixed target operation, the compensation is designed for an intensity of $6x10^{10}$ per bunch with a ramp rate of 240 GeV/sec. The maximum intensity that could be accelerated at this ramp rate without running into instabilities is not much larger, perhaps $7x10^{10}$. The most critical beam loading compensation is necessary for snap coalescing twelve batches of protons at 150 GeV.

5.9 Intensity and Transmission Efficiency

The Fermilab Main Injector is designed to have a much larger aperture, greater than 40π mm-mr normalized at 8 GeV, compared to the Main Ring aperture of 12π mm-mr. The Main Ring aperture, both transverse and longitudinal, limits the performance of the Fermilab Tevatron complex. The Main Ring is not capable of efficiently accelerating the full intensity that will be available from the Booster, namely 6×10^{10} protons/bunch. The Main Ring is used in three different modes: 1) proton acceleration from 8 GeV to 120 GeV for antiproton production; 2) proton acceleration from 8 GeV to 150 GeV, coalescing and cogging for Tevatron injection; and 3) antiproton acceleration from 8 GeV to 150 GeV, coalescing and cogging for Tevatron injection. In the first two modes the Main Ring accepts beam from the Booster, and in the third mode from the Antiproton Source. In all of these modes the beam intensity is limited by the admittance of the Main Ring, and furthermore, the Main Ring has no transverse aperture left for any motion in orbit.

In the antiproton production mode the Booster runs with 84 bunches of about $4.5x10^{10}$ protons each. Main Ring delivers only about $3.5x10^{10}$ protons/bunch to the antiproton production target, with an efficiency of less than 80%. Figure 5.14 shows the efficiency of proton transfer through the Main Ring for different Main Ring cycles. In the Main Ring about 10% of particles get lost in the first few thousand turns. This loss is mainly caused by the small aperture of the Main Ring at injection. The small aperture is caused by a combination of poor magnetic field quality at low excitation and perturbations to the ring that have been required for the integration of overpasses and new injection and extraction systems. The second considerable loss of particles in the Main Ring, about 10%, is at transition energy. At transition the growing beam size also scrapes on the limited aperture of the Main Ring. Figure 5.14 also shows the transfer efficiencies for the other two cycles of the Main Ring operation, which are used to fill the Tevatron for collider operations. As in the antiproton production cycle, these two cycles have losses of particles from injection to transition energy. The total loss is about 20%. A few percent (<3%) of particles get lost between 20 GeV and 150 GeV. Due to the limited momentum aperture of the Main Ring, the proton loss during cogging and coalescing is about 25%. *The average transmission through the Main Ring during antiproton production cycles is at best 80%, whereas the average transmissions of coalesced proton and antiproton bunches are 50% and 70% respectively.* The antiproton transmission is larger due to the smaller emittance of the antiproton beam from the Accumulator.

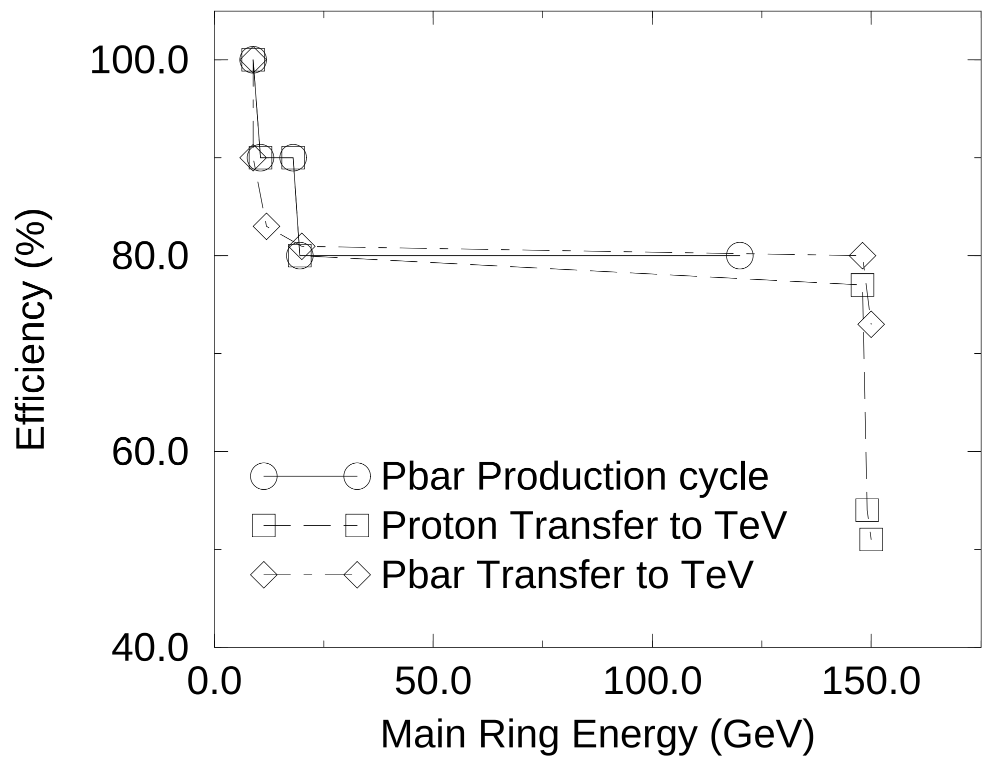

Figure 5.14. Main Ring transmission efficiencies for different particle transfer cycles.

In the Main Injector era, the Booster proton emittance is expected to be about 18π mm-mr for $6x10^{10}$ protons/bunch. The Main Injector, with an aperture more than three times larger than the Main Ring, will eliminate most of the losses currently caused by the aperture restrictions at injection. Any loss due to small injection oscillations will also be reduced. Figure 5.15 shows the expected particle transmission for different Main Injector cycles. Due to much larger transverse admittance of the Main Injector, the expected loss from injection to transition energy is less than 5%. The Main Injector is designed to have larger momentum aperture; hence loss of particles at cogging and coalescing is expected to be much smaller than in the Main Ring. A conservative estimate of these losses is less than 5%. The average transmission through Main Injector during antiproton production cycles is expected to be 95%. The average transmission efficiencies of coalesced proton and antiproton bunches are expected to be 85% and 90% respectively. The Main Injector is designed to exceed the Run II requirements of $2.7x10^{11}$ protons/bunch and $5.5x10^{10}$ antiproton/bunch delivered to the Tevatron.

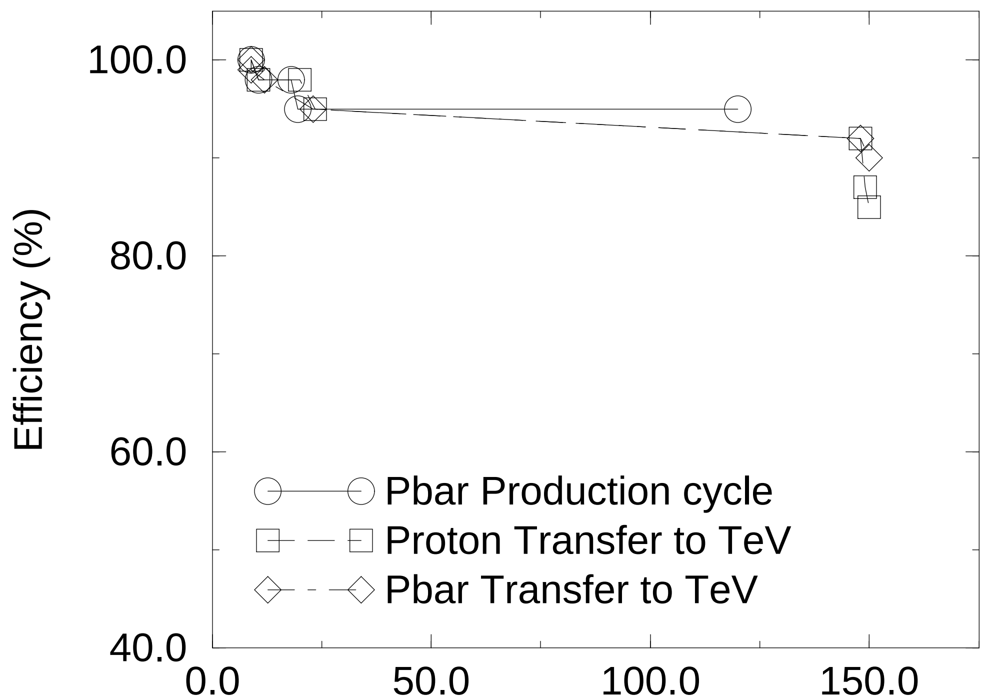

Figure 5.15. Expected Main Injector transmission efficiencies for different particle transfer cycles.

5.10 Resonant Extraction

The Main Injector slow extraction system is designed to be capable of providing year-round, uniform spills of 120 GeV beams, either with a 2.9 s cycle time and 1 s flattop, or with a 1.9 s cycle time and ~1 ms spill for neutrino experiments. The following sections outline the principle of slow spill through excitation of the half-integer resonance, and description of the hardware required. More detail is provided in the TDH on results from numerical simulation of the extraction process, and on spill modulation and duty factor considerations.

5.10.1 Half-Integer Resonant Extraction

The half-integer resonance is a linear resonance that can be induced solely by a quadrupole field. In that case, the beam is either entirely stable or entirely unstable, if tune spread resulting from chromaticity and momentum spread is ignored. With the addition of an octupole field, however, an amplitude-dependent tune spread is introduced into the beam ($\Delta\nu \sim x^2$). Particles with large betatron amplitudes have tunes closer to the half-integer than those of small amplitude. Consequently, the phase space splits into stable and unstable regions, thereby providing a means for manipulating the extraction rate through control of the stable area in phase space. Recycled Main Ring octupoles distributed around the ring on the 0th-harmonic provide the non-linear tune shift, while two orthogonal families of Main Ring trim quads distributed on the 53rd-harmonic provide the half-integer driving term. One quadrupole family alone produces the desired driving term for extraction, while both families are available for correcting the intrinsic half-integer stop-band of the machine.

Slow extraction from the Main Injector proceeds basically as follows. The horizontal tune is raised towards the half-integer from $\nu_x = 26.425$ to 26.485 using the main quadrupole circuits. The desired orientation of the phase-space at the extraction septa is obtained by energizing the appropriate 53rd-harmonic quadrupole circuit plus the 0th-harmonic octupoles. The strengths of the harmonic elements are chosen such that the stable phase-space area equals the emittance of the circulating beam. The beam is just marginally stable, therefore, at the end of the initial ramp.

Extraction begins by further ramping the harmonic quadrupoles to increase the width of the half-integer stop-band and start the stop-band moving through the beam. Small amplitude particles (lower tune) remain stable, with their motion in phase-space oscillating between the 'fixed' points on successive turns. As the stable phase-space region shrinks, large amplitude particles enter the stop-band and become unstable, with their amplitude then growing exponentially from turn to turn. The unstable particles stream out along the separatrices until they ultimately jump across (or hit) the wires of the electrostatic septa and enter the extraction channel. The kick supplied by the electrostatic septa provides sufficient separation between extracted and circulating beams that magnetic septa are used for the final extraction from the machine.

5.10.2 Extraction Elements

There are five major components of the resonant extraction system:

1. magnetic and electrostatic extraction septa;
2. one family of 0th-harmonic octupoles;
3. two families (cosine and sine) of 53rd-harmonic quadrupoles;
4. low frequency extraction regulation quadrupoles (QXR), and;
5. high frequency spill modulation regulation quadrupoles (Buckers).

The extraction septa are located in straight section MI-52 for extraction to Switchyard and the present experimental areas beyond. This region must accommodate extraction of 120 GeV/c slow-spill protons and single-turn extraction of 120 and 150 GeV/c protons. The Lambertson magnetic septa and C-magnets are common to all beam transfers. There is sufficient phase advance in the straight section that both the extraction kicker magnets and electrostatic septa can be placed at the upstream end of the straight section. Separation between extracted and circulating beams is provided by three electrostatic septum modules located immediately downstream of the kickers, and 70.1° in betatron phase upstream of the entrance to the first Lambertson. Each septum has a wire plane length of 3.048 m. The high voltage gap is 10 mm, with the anode consisting of 0.1 mm tungsten-rhenium wires. The septa are designed to produce 200 μr of kick each at an applied voltage gradient of 79 kV/cm. Additional septa and Lambertsons are required in MI-60 for extracting to NUMI. Due to the presence of the rf cavities in the MI-60 straight section, the electrostatic septa will be located ~$3\pi/2$ in phase advance ahead of the first Lambertson magnet.

The 0th-harmonic octupole circuit is required to serve two functions. During resonant extraction it augments the (large) octupole component of the main quadrupoles to produce the appropriate stable and unstable phase-space regions. At injection, however, the octupole field generated by the main quads has a degrading effect on dynamic aperture. The harmonic octupoles in this case are used to cancel this detuning effect. The Main Injector has a single family of 54 octupoles - one at each focusing sextupole location. All octupoles are the same polarity, producing a 0th-harmonic contribution. The two-fold symmetry of the Injector ensures that half-integer driving terms cancel, and quarter-integer harmonics are found to be small.

The number of harmonic quadrupoles is determined by the strength required to raise the fractional horizontal tune from 0.485 to 0.500 at 120 GeV/c. With β_x ~ 50 m at the quadrupole locations, the total strength required is ~15 kG-m/m. For Main Ring trim quads this translates into 8 quadrupoles operating at ~7 A. In the Main Injector 16 quadrupoles are utilized. These are distributed around the ring, separated into two orthogonal families (cosine and sine) of eight quads each. Within each family 0th-harmonic contributions cancel because there are equal numbers of F and D quads. The 53rd-harmonic is retained by separating opposite polarity quads by odd multiples of 90° in betatron phase. The orthogonality of the families provides the capability both to cancel the intrinsic half-integer stop-band of the machine and to manipulate the orientation of the phase-space at the septa if necessary for extraction either at MI-52 or at MI-60.

Quadrupole errors in the ring propagate at twice the tune and contribute an additional (unwanted) half-integer driving term. The intrinsic half-integer stop-band is measured by ramping the two orthogonal families independently through positive and negative current values to attain resonance. In the absence of dynamic non-linearities the four resonant current values lie on the circumference of a circle. The circle center defines the stop-band width and phase and, therefore, the harmonic quad currents necessary to cancel it. The stop-band compensation is required to reduce the large variations in the Main Injector lattice functions. The maximum $\Delta\beta/\beta$ is reduced from 76% to 6%, and the rms deviation from 41% to just 3%. To a good approximation the design lattice is obtained.

5.10.3 Spill Regulation Elements

The spill regulation for extraction system can be divided functionally into two bandwidths.

1. A low bandwidth (dc to ~10 Hz) system, commonly called QXR, or quadrupole extraction regulation system, consists of two air-core quadrupoles, which may be configured either as a 0th-harmonic or as a 53rd-harmonic. Further analysis is being done to determine which mode is preferred. QXR is used to control the rate at which the beam is extracted. The system is regulated with feed-forward by monitoring the circulating beam intensity during slow extraction. On each machine cycle, the spill rate is sampled at 720 Hz, and compared to the desired spill rate. The error is saved, smoothed and time-shifted, and the current wave form for the next cycle is modified based on an average over many previous cycles.

2. A higher bandwidth (0.1 Hz to 3 kHz) system consists of two air-core, 0th-harmonic quadrupoles powered in series, mounted on ceramic beam pipe. These are commonly referred to as "buckers." By sampling the extracted beam intensity at 5760 Hz and through feed-forward to the buckers, higher-frequency repetitive spill modulation is removed. Real-time feedback is also applied, limited in bandwidth to a few hundred Hz due to the time delay between a change in quadrupole current and the beam response. Simulations have demonstrated that this system can compensate for 100 ppm ripple at 360 Hz in the main quadrupole bus, corresponding to tune modulation of $\Delta\nu \sim \pm 0.003$. Ripple in the main quadrupole bus could also be compensated by feeding back directly into the bucker system.

The 12-year-old Tevatron extraction regulation systems was recently redesigned using modern technology. Much of the Tevatron extraction system, especially in the area of software and controls, will be carried over directly to the Main Injector QXR system.

---

[1] M.J. Syphers, "Injection Mismatch and Phase Space Dilution", FN-458, 1987.
[2] *The Fermilab Main Injector Technical Design Handbook*, Section: 2.4, 1994.